

pubs.acs.org/est Article

Superoxide Formation from Aqueous Reactions of Biogenic Secondary Organic Aerosols

Jinlai Wei, Ting Fang, Cynthia Wong, Pascale S. J. Lakey, Sergey A. Nizkorodov, and Manabu Shiraiwa*



Cite This: Environ. Sci. Technol. 2021, 55, 260-270



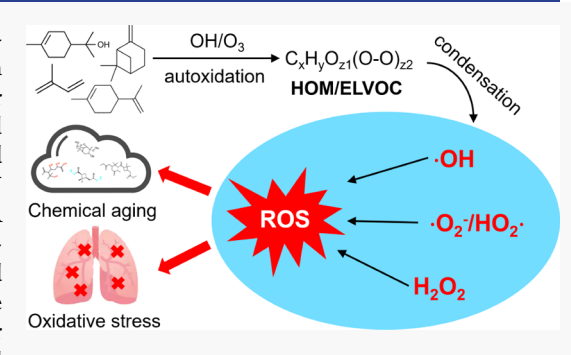
ACCESS

Metrics & More

Article Recommendations

Supporting Information

ABSTRACT: Reactive oxygen species (ROS) play a central role in aqueous-phase processing and health effects of atmospheric aerosols. Although hydroxyl radical (${}^{\bullet}$ OH) and hydrogen peroxide (H_2O_2) are regarded as major oxidants associated with secondary organic aerosols (SOA), the kinetics and reaction mechanisms of superoxide ($O_2^{\bullet-}$) formation are rarely quantified and poorly understood. Here, we demonstrate a dominant formation of $O_2^{\bullet-}$ with molar yields of 0.01–0.03% from aqueous reactions of biogenic SOA generated by ${}^{\bullet}$ OH photooxidation of isoprene, β-pinene, α-terpineol, and D-limonene. The temporal evolution of ${}^{\bullet}$ OH and $O_2^{\bullet-}$ formation is elucidated by kinetic modeling with a cascade of aqueous reactions including the decomposition of organic hydroperoxides, ${}^{\bullet}$ OH oxidation of primary or secondary alcohols, and unimolecular decomposition of α-hydroxyperoxyl



radicals. Relative yields of various types of ROS reflect a relative abundance of organic hydroperoxides and alcohols contained in SOA. These findings and mechanistic understanding have important implications on the atmospheric fate of SOA and particle-phase reactions of highly oxygenated organic molecules as well as oxidative stress upon respiratory deposition.

■ INTRODUCTION

Secondary organic aerosols (SOA) constitute a major fraction of ambient particulate matter and have significant impacts on global climate, air quality, and public health. 1,2 Biogenic volatile organic compounds (VOCs), including isoprene and monoterpenes, have been identified as the primary precursors of SOA around the globe,3 including the Amazon region,4 China,⁵ and southeastern United States.⁶ The formation of SOA is initiated by multigenerational oxidation of VOCs and subsequent condensation of semivolatile oxidation products.^{3,7} Recent studies have revealed that highly oxygenated organic molecules (HOMs) and low volatility organic compounds generated by autoxidation substantially contribute to new particle formation and SOA growth.^{8,9} These compounds are found to be labile in the particle phase 10 and a recent study suggested that particle-phase reactions need to be considered for full understanding of the atmospheric fate of HOMs. 11 Particle-phase chemistry and aqueous-phase processing involving oxidants and water-soluble organic compounds in cloud and fog droplets are very efficient pathways for the chemical transformation of SOA. 12-14 These aging processes can lead to the change of particle properties including cloud condensation nuclei activity¹⁵ and absorption coefficient because of the formation of light-absorbing compounds.¹⁶

Reactive oxygen species (ROS), including the hydroxyl radical (${}^{\bullet}OH$), superoxide ($O_2{}^{\bullet-}$), hydroperoxyl radical (HO_2^{\bullet}), and hydrogen peroxide (H_2O_2), play a central role in chemical transformation of organic and inorganic compounds in the atmosphere. ¹⁷ Substantial amounts of H_2O_2

were detected in ambient and laboratory-generated SOA, resulting from the hydrolysis of hydroxyhydroperoxides and peracids. 18,19 OH, the most reactive form of ROS, was found to be released by decomposition of organic hydroperoxides, ²⁰ peracids, 21 and HOMs. 22 Although OH and H2O2 have been traditionally considered as the most important oxidants in aqueous droplets and thus studied extensively, additional oxidants have received growing attention. Singlet oxygen and organic triplet-excited state have emerged as new oxidants produced from dissolved organic compounds in atmospheric water.^{23,24} Redox reactions of quinones contained in aromatic SOA can lead to the formation of $O_2^{\bullet-25,26}$ Previous studies have observed O2 •- formation from biogenic-ozonolysis SOA as a minor component; 20,26-28 however, the mechanism and kinetics of O2 • formation are poorly understood and rarely quantified.

Ambient SOA are found to have significant oxidative potential, which can be correlated with the formation of H_2O_2 and $O_2^{\bullet-}$ in epithelial-lining fluid, inducing oxidative stress and adverse health effects upon inhalation and deposition in the human respiratory tract. ROS can

Received: November 17, 2020 Revised: December 2, 2020 Accepted: December 10, 2020 Published: December 22, 2020





exert drastic effects on biological tissues and cell components, subsequently causing acute airway inflammation and cardio-pulmonary illnesses. 31,33 Low levels of $O_2^{\bullet-}$ modulate various kinases or directly activate transcription factors to affect gene regulation in the nucleus; ³⁴ however, excess $O_2^{\bullet-}$ formation is cytotoxic and induces a variety of diseases. ³⁵ $O_2^{\bullet-}$ is also known as a crucial precursor of H2O2, which can be further converted via Fenton (-like) reactions into OH. 32,36 Given the atmospheric and physiological importance of ROS, it is critical to quantify kinetics and elucidate chemical mechanisms of the formation of different types of ROS from SOA in the aqueous phase. In this study, we observe substantial formation of O₂•by the SOA formed by ${}^{\bullet}$ OH photooxidation of isoprene, β pinene, α -terpineol, and D-limonene with the highest formation efficiency for the α -terpineol SOA. We found that the oxidation pathways (e.g., ozonolysis vs *OH photooxidation) and chemical composition of SOA play a critical role in determining ROS composition. Using a combination of laboratory experiments and kinetic modeling, we demonstrated that $O_2^{\bullet-}$ formation is caused by a cascade of aqueous reactions of biogenic SOA, involving the decomposition of organic hydroperoxides, OH oxidation of primary or secondary alcohols, and unimolecular decomposition of α hydroxyperoxyl radicals. To the best of our knowledge, this is the first study that explicitly addresses the mechanisms and kinetics of O2 - formation from biogenic SOA involving aqueous chemistry. These results have significant implications on chemical transformation of organic compounds in the atmosphere and adverse aerosol health effects in the human respiratory tract.

MATERIALS AND METHODS

SOA Formation, Collection, and Extraction. SOA particles were generated from dark ozonolysis and OH photooxidation (referred as SOA_{O3} and SOA_{OH}, respectively) of isoprene (Sigma-Aldrich, \geq 99%), β -pinene (Sigma-Aldrich, \geq 99%), α -terpineol (Arcos Organics, 97%), and D-limonene (Arcos Organics, 96%). Figure S1 shows the schematics of both oxidation systems. Briefly, SOA_{O3} particles were produced in an oxidation flow reactor under dry and dark conditions. Prior to each experiment, the reactor was purged with zero air (Parker 75-62 purge gas generator). Ozone was introduced into the reactor by flowing pure oxygen at 1 standard liter per minute (slm) through a commercial ozone generator (OzoneTech OZ2SS-SS). After the ozone concentration was stabilized, pure isoprene, β -pinene, α -terpineol, and D-limonene were injected into 5 slm of purge air flow separately using a syringe pump at a rate of \sim 2 μ L per minute. High concentrations $(2.2 \times 10^{15} \text{ cm}^{-3} \text{ for isoprene and})$ $1.4 \times 10^{15} \text{ cm}^{-3}$ for β -pinene, α -terpineol, and D-limonene) of precursor and ozone $(1.8 \times 10^{14} \text{ cm}^{-3})$ were used to generate enough materials for analysis.

SOA_{OH} particles were generated in a 19 L potential aerosol mass (PAM) reactor. 37 100–500 μ L of VOC precursors (isoprene, β -pinene, α -terpineol, and p-limonene) were placed in an open 1.5 mL amber glass vial, which was kept inside a glass bottle prior to the PAM reactor. The precursors were then injected into the chamber using a 0.5 slm of carrier flow mixed with a 6 slm of humidified (Perma Pure humidifier, MH-110-12P-4) flow of purified air from a zero-air generator (model 7000, Environics). The *OH was generated through photolysis of water molecules by 185 nm UV radiation. The exposure time for the photooxidation of precursors in the PAM

reactor was about 3 min with a relative humidity around 30-40%. Despite the high *OH concentrations ($\sim 10^{11}-10^{12}$ cm⁻³) compared to ambient levels ($\sim 10^6$ cm⁻³), the PAM-generated SOA are found to be similar to ambient and chamber-generated SOA in terms of yield, oxidation state, hygroscopicity, and chemical composition. ^{38–40} Additional advantages of the PAM reactor include shortened experimental timescales, ability to reach long photochemical ages, and minimized wall losses. ⁴⁰

A scanning mobility particle sizer (SMPS, Grimm Aerosol Technik) was used to record the number concentrations and size distributions of SOA produced in the PAM reactor. The typical particle diameter of SOA_{OH} ranged from 30 to 500 nm, and the geometric mean diameter by mass varied from 70 to 120 nm. Particle sampling was initiated after the number concentrations stabilized. The SOA particles were collected on 47 mm-polytetrafluoroethylene filters (Millipore FGLP04700, 0.2 μ m pore size) at a flow rate of 13 slm for 40 min and 5 slm for 3 h for SOA_{O3} and SOA_{OH} , respectively.

The filter samples were extracted in 1 mL spin-trapping solutions (10 mM) or Milli-Q (deionized, resistivity = 18.2 $M\Omega/cm$) water for 7 min. The filter extracts were used for radical measurements or the H_2O_2 fluorometric assay, respectively. The mass difference before and after the extraction was regarded as the SOA dissolved in reagents, and an average molar mass of 200 g mol $^{-1}$ was used for calculating the SOA molar concentrations in filter extracts. The SOA_{O3} and SOA_{OH} concentrations were in the range of 1–16 mM and pH of SOA extracts varied between 4 and 6. At least three samples were prepared for each SOA_{O3} and SOA_{OH} for EPR analysis and H_2O_2 measurement, respectively.

EPR Measurements. A continuous-wave electron paramagnetic resonance (CW-EPR) spectrometer (Bruker, Germany) coupled with a spin-trapping technique was used for free radical quantification. The spin-trapping agent used to capture free radicals generated upon aqueous reactions of SOA is 5-tert-Butoxycarbonyl-5-methyl-1-pyrroline-N-oxide (BMPO) (Enzo, \geq 99%). After extraction, the filter extracts were incubated at a room temperature of 20 $^{\circ}\text{C}\text{,}$ and a 50 μL aliquot was loaded into a 50 μ L capillary tube (VWR) and inserted in the resonator of the EPR spectrometer at 10, 20, 60, 120, and 240 min from the start of aqueous reactions. The parameter sets for EPR measurements were a center field of 3515.0 G, a sweep width of 100.0 G, a receiver gain of 30 dB, a modulation amplitude of 1.0 G, a scan number of 10-50, attenuation of 12 dB, a microwave power of 12.6 mW, a modulation frequency of 100 kHz, and a conversion time/time constant of 5.12 ms. After obtaining the EPR spectra, SpinFit and SpinCount methods embedded in the Bruker Xenon software were applied to quantify BMPO-radical adducts²⁰ at each time point.

H₂O₂ Fluorometric Assay. A modified protocol⁴¹ was applied for the H_2O_2 measurement using a fluorometric H_2O_2 assay kit (MAK165, Sigma-Aldrich). 250 μ L of DMSO and 1 mL of assay buffer were added to the red peroxidase substrate and horseradish peroxidase for reconstitution, respectively. The reagents were divided into ten sets of aliquots (25 μ L of red peroxidase substrate, 100 μ L of horseradish peroxidase, and 2 mL of assay buffer each). Prior to each analysis, one set of reagents was used to prepare 2 mL working solutions, consisting of 20 μ L of red peroxidase substrate, 80 μ L of horseradish peroxidase, and 1.9 mL of assay buffer. All H_2O_2 measurements were conducted within 2 h from the preparation

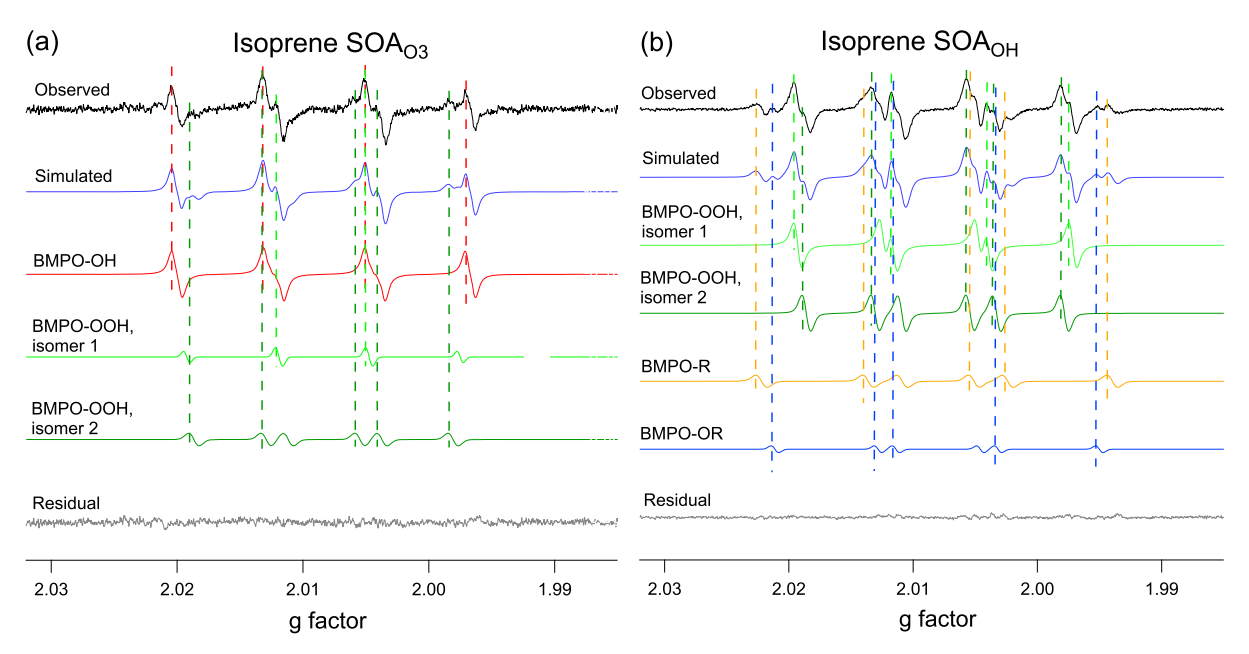


Figure 1. EPR spectra of BMPO-radical adducts from aqueous reactions of isoprene SOA generated from (a) dark ozonolysis and (b) OH photooxidation. The observed spectra (black) are simulated (purple) and deconvoluted into BMPO-OH (red), BMPO-OOH isomer 1 (light green), BMPO-OOH isomer 2 (dark green), BMPO-R (yellow), and BMPO-OR (blue). Residual (gray) denotes the difference of observed and simulated spectra. Note that the two isomers of BMPO-OOH represent the trans or cis structures of the -OOH group.

of working solutions because of the high instability of the probe. A calibration was performed using H2O2 standard concentrations ranging from 0.05 to 1.5 µM, which were prepared by diluting 30 wt % H₂O₂ (Sigma-Aldrich). The reaction vials (3 mL) consisted of 2.94 mL of solution (Milli-Q water + filter extracts) and 60 μ L of working solution. The H₂O₂ yields from different SOA samples varied significantly and dilution factors were adjusted, so that the final H₂O₂ concentrations in the reaction vials were below 1.5 μ M. All H₂O₂ measurements were conducted with a filter blank, with the same dilution factor as the samples. The addition of working solution was considered as the start of reaction, and the reaction vials were incubated at room temperature for 15 min until the measurement. The fluorescence of the reagents was measured using a spectrofluorophotometer (RF-6000, Shimadzu) at excitation and emission wavelengths of 540 and 590 nm, respectively.

Kinetic Modeling. A kinetic model was applied to simulate the simultaneous formation of OH and O2 -/HO2 by aqueous reactions of SOA using the reactions listed in Table S2. The reactions include chemical reactions of SOA components (R1-R7), ROS coupling reactions (R8-R16), and radical-trapping reactions by BMPO (R17-R21). SOA chemistry includes decomposition of organic hydroperoxides (ROOH), generating *OH radicals (R1), 20,26 *OH oxidation of primary and secondary alcohols (R1R2CHOH) and subsequent reaction with O_2 to form α -hydroxyperoxyl radicals $(R_1R_2C(O_2)OH^{\bullet})$ (R2), decomposition of $R_1R_2C(O_2)OH^{\bullet}$ to generate HO_2^{\bullet} (R3), 42,43 $^{\bullet}OH$ oxidation of ROOH (R4),42 R₁R₂C(O₂)OH• (R5), and other SOA components (R6) and HO_2^{\bullet} termination of $R_1R_2C(O_2)OH^{\bullet}$ (R7). The reaction yield of R3 (c_1) was also considered in the model. Rate coefficients of the decomposition of ROOH and R1R2C(O2)OH as well as H-abstraction of R₁R₂CHOH were assumed to be independent of the structures of R groups contained among different SOA, representing a major model assumption. This assumption is in line with the CAPRAM 3.0 model, 42 in which

the rate constants of H-abstraction on alcohols vary within one order of magnitude regardless of carbon numbers and functionalities besides the hydroxy group. The radical composition profiles generated by different SOA are solely determined by the relative abundance of ROOH and $R_1R_2\mbox{CHOH}$ groups in SOA. Potential variation of these rate constants depending on R structures can be partly translated into uncertainties in molar fractions of ROOH and $R_1R_2\mbox{CHOH}$ as shown in Table S3.

The rate coefficients of ROS coupling reactions were obtained from literature values and the unknown rate coefficients and molar fractions of ROOH and R₁R₂CHOH contained in SOA were determined using the Monte Carlo genetic algorithm (MCGA) to reproduce experimental data. 44 In the Monte Carlo search, input parameters were varied randomly within individual bounds: the boundaries of all reaction rate constants were generally constrained to within two orders of magnitude based on literature studies, while the ROOH/R₁R₂CHOH molar fractions were constrained to between 0.1 and 80%. As discussed in the main text, the determined rate coefficients and molar fractions are reasonable and in line with previous experimental measurements and modeling studies. The uncertainty of the reaction rates in Table S2 and the ROOH/R₁R₂CHOH fractions in Table S3 were obtained by running the MCGA numerous times (\sim 40), which resulted in 20 parameter sets which reasonably captured the temporal trends of the experimental data. The 20 parameter sets were then used to plot 20 traces for the temporal formation of the BMPO adducts by each SOA, and the highest and lowest traces were selected as the upper and lower boundaries shown in Figure 3 for each SOA, respectively. Note that these boundaries do not necessarily correspond to the boundaries of each parameter in Tables S2 and S3. There is still relatively large uncertainty in the actual values of some parameters, as shown by the parameter ranges in Table S2; further measurements to quantify organic hydroperoxides and alcohols as well as dedicated kinetic

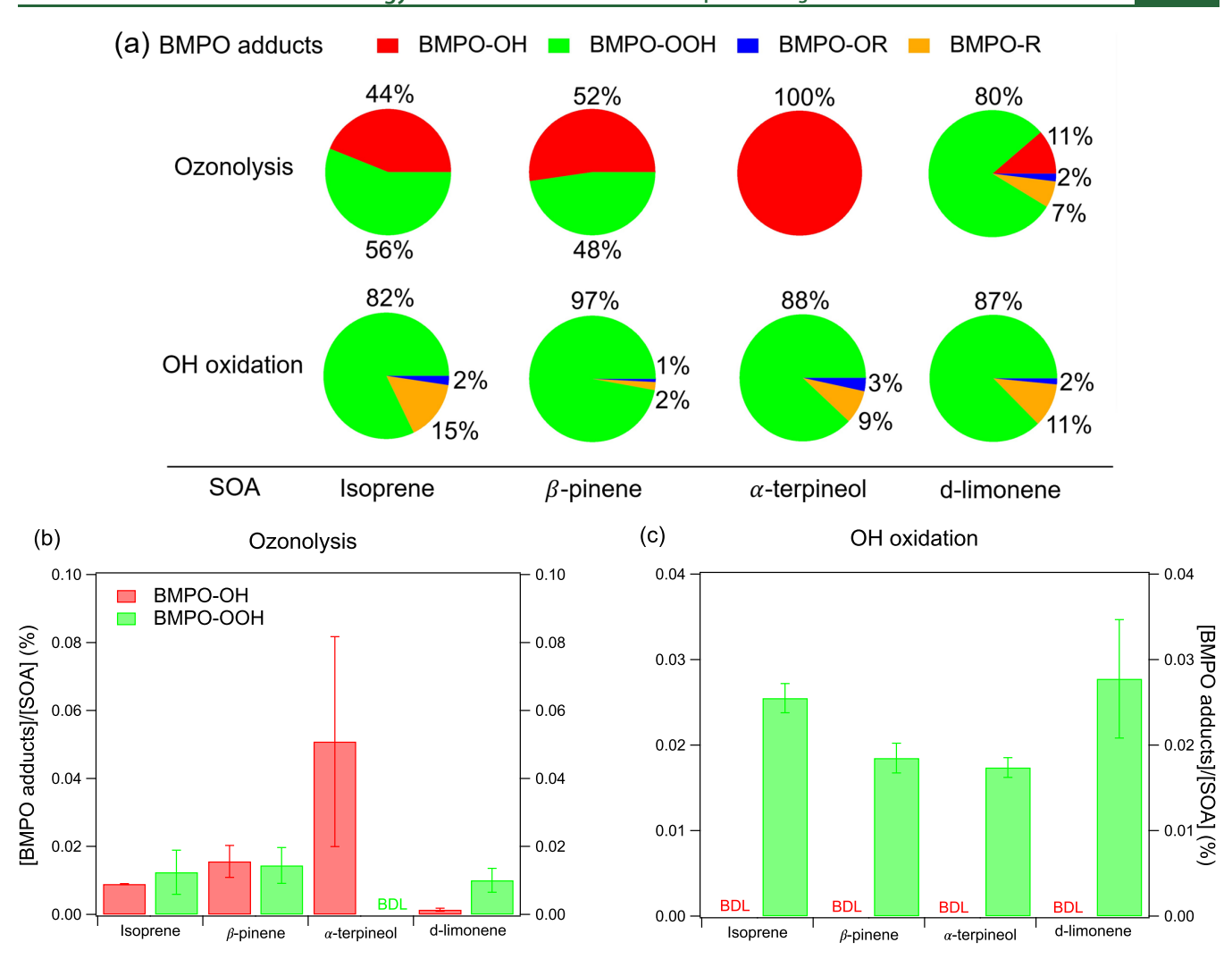


Figure 2. (a) Relative yields of BMPO-radical adduct from aqueous reactions of SOA generated by ozonolysis vs $^{\bullet}$ OH photooxidation of isoprene, β -pinene, α -terpineol, and D-limonene. Molar yields of BMPO-OH (red) and BMPO-OOH (green) adducts generated by SOA from (b) dark ozonolysis and (c) $^{\bullet}$ OH photooxidation after 20 min of aqueous reactions.

studies would be required for determination of these parameters.

The relative abundance of $O_2^{\bullet-}$ and HO_2^{\bullet} in the aqueous solution is largely determined by pH. Tresp et al. 45 showed that at neutral pH (7.4), over 99.9% of BMPO-OOH was generated by BMPO reacting with O₂•-. In contrast, the pH of the SOA aqueous solutions obtained in this study ranged from 4 to 6. According to the Henderson-Hasselbalch equation with a p K_a value of 4.88 for HO_2^{\bullet} , HO_2^{\bullet} would dominate over $O_2^{\bullet-}$ when the pH approaches 4, while $O_2^{\bullet-}$ and HO_2^{\bullet} are in comparable amounts when the pH = \sim 5. Therefore, BMPO trapping reactions of both $O_2^{\bullet-}$ and HO_2^{\bullet} to form BMPO-OOH are considered (R18, 19).²⁸ The BMPO radical adducts (BMPO-OH, BMPO-OOH) can decay by self-decomposition or reactions with other radicals. Although self-decomposition half-life of BMPO-OH and BMPO-OOH in neutral solutions are known to be 30 min⁴⁶ and 23 min,⁴⁷ respectively, rate coefficients with radicals (e.g., OH, O2 -, organic radicals) leading to adduct decay are unknown. Thus, in this study, decay of BMPO-OH (R18) and BMPO-OOH (R21) are treated with pseudo-first-order rate coefficients. The estimated half-lives of BMPO-OH and BMPO-OOH are shorter than the literature values to be 14-24 min and 6-14 min, respectively,

indicating that decay of adducts by radicals are nonnegligible or lower pH may have impacted adduct stability. 48

■ RESULTS AND DISCUSSION

ROS Formation Efficiencies by SOA. Biogenic SOA were generated by both dark ozonolysis and *OH photooxidation (referred as SOA_{O3} and SOA_{OH} hereafter) of isoprene, β pinene, α-terpineol, and D-limonene. Particle water extracts were analyzed with electron paramagnetic resonance (EPR) spectroscopy coupled with a spin-trapping technique for the detection of free radicals. Figure 1 shows the observed EPR spectra of isoprene (a) SOA_{O3} and (b) SOA_{OH}. The observed spectra were simulated and deconvoluted into spectra for different BMPO adducts with radicals including OH, O2 O-/ HO2, and carbon- and oxygen-centered organic radicals (BMPO-OH, BMPO-OOH, BMPO-R, and BMPO-OR, respectively). The EPR spectrum of isoprene SOA_{O3} is dominated by a four-peak pattern, which can be attributed to BMPO-OH with a minor contribution from BMPO-OOH. In contrast, the major peaks in the EPR spectrum from isoprene SOA_{OH} represent BMPO-OOH with a minor contribution from carbon- and oxygen-centered organic radicals. Similar trends are observed for β -pinene and α -terpineol SOA, while D-

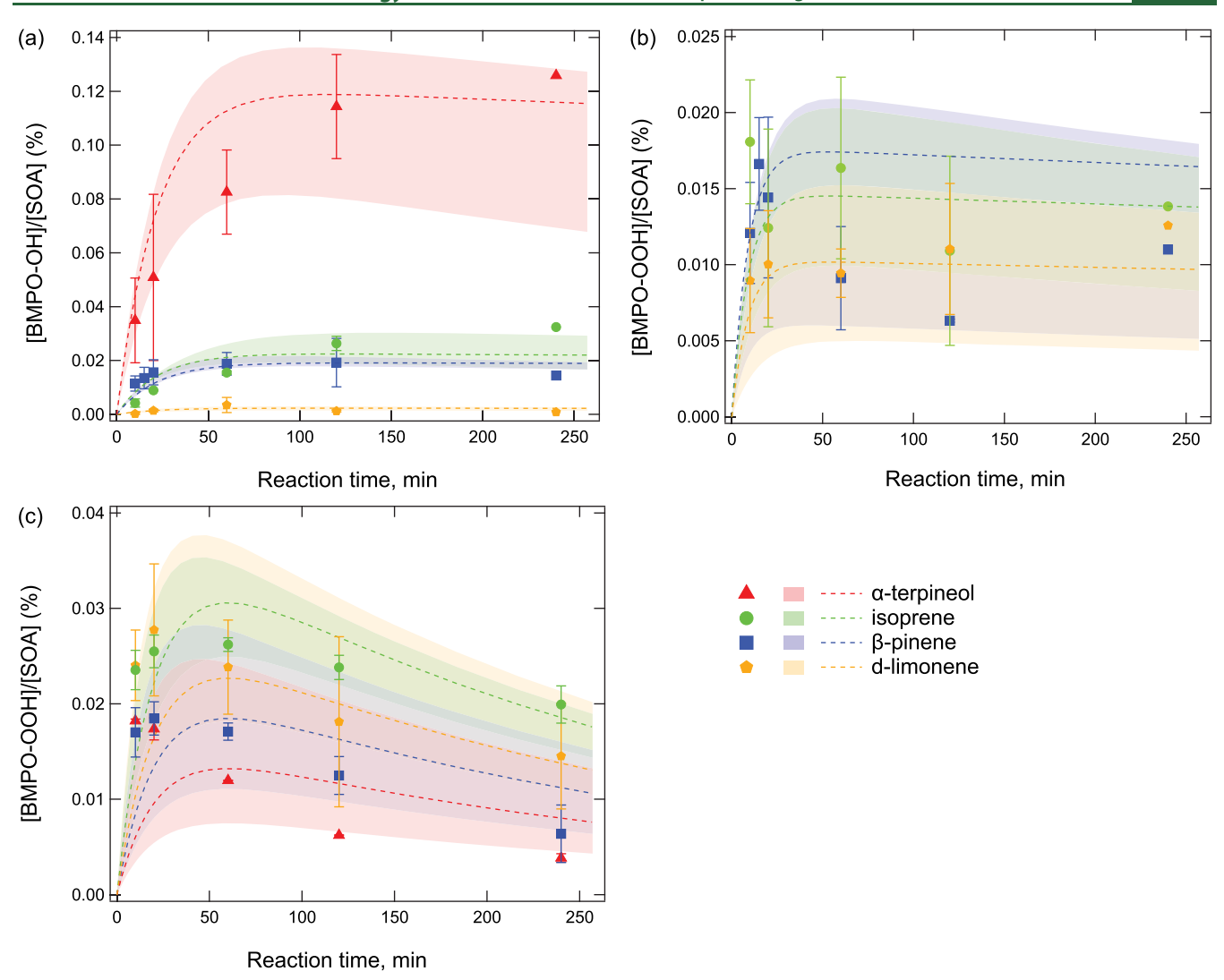


Figure 3. Temporal evolution of molar yields of (a) BMPO-OH and (b) BMPO-OOH adducts from aqueous reactions of SOA generated from dark ozonolysis (SOA_{O3}) and (c) BMPO-OOH adducts from SOA generated from ${}^{\bullet}$ OH photooxidation (SOA_{OH}) of α-terpineol (red), isoprene (green), β-pinene (blue), and p-limonene (yellow). The markers are experimental data. The dashed lines represent the best fits of kinetic model with the shaded area denoting the modeling uncertainties. The $O_2^{\bullet-}/HO_2^{\bullet}$ formation from α-terpineol SOA_{O3} and ${}^{\bullet}$ OH formation from all SOA_{OH} are below the detection limit.

limonene SOA mainly produces $O_2^{\bullet-}/HO_2^{\bullet}$ for both oxidation systems (Figure S2).

Integration of deconvoluted spectra allows us to quantify contributions from each radical species. Figure 2 shows quantifications of different types of radicals in water extracts of the SOA generated by ozonolysis or *OH oxidation of isoprene, β -pinene, α -terpineol, and D-limonene. Relative yields of BMPO-OH of isoprene and β -pinene SOA_{O3} after 20 min of reactions are 44 and 52%, respectively (Figure 2a), both of which further increase to >70% after 2 h (Figure S3a). This is in very good agreement with a previous study which demonstrated major OH formation from biogenic SOA formed by ozonolysis. The α -terpineol SOA_{O3} generates OH exclusively, while the D-limonene SOA_{O3} generates O₂•-/ HO₂ dominantly (80%) with minor contributions from OH (11%) and organic radicals (7%). In contrast to major OH formation by most of SOA_{O3}, more than 80% of radical species generated from SOA_{OH} are in the form of O₂•-/HO₂•. Figure 2b,c shows the molar yields or formation efficiencies of OH and O2 • -/HO2 (molar concentration ratios of BMPO-radical

adduct to SOA) for SOA $_{O3}$ and SOA $_{OH}$, respectively. α -Terpineol SOA $_{O3}$ has the highest $^{\bullet}$ OH formation efficiency with 0.06% followed by β -pinene and isoprene SOA $_{O3}$. All types of SOA $_{OH}$ are found to have a similar O $_2^{\bullet-}/HO_2^{\bullet}$ formation efficiency of 0.018-0.03%.

The molar yields of H_2O_2 from SOA were also quantified using a fluorometric H_2O_2 assay (Table S1). Isoprene SOA generally yields higher H_2O_2 compared to other types of SOA. The H_2O_2 yield from β -pinene SOA $_{O3}$ (1.8 \pm 0.3%) is comparable with results of Wang et al. (1.3 \pm 0.9%), 18 but around half of the amount reported by Tong et al. (3.2 \pm 0.7%). 26 Isoprene SOA $_{O3}$ generally produces higher H_2O_2 (4.2 \pm 0.7%) compared to β -pinene SOA $_{O3}$ (1.8 \pm 0.3%), which are comparable with Tong et al. 26 (8.0 \pm 0.8% for isoprene SOA $_{O3}$ and 3.2 \pm 0.7% for β -pinene SOA $_{O3}$). For both oxidation systems with various precursors, the production of $O_2^{\bullet-}/HO_2^{\bullet}$ is tightly correlated with H_2O_2 formation with R^2 greater than 0.9 (Figure S4), indicating that $O_2^{\bullet-}$ is an important precursor of H_2O_2 , or $O_2^{\bullet-}$ and H_2O_2 have similar types of source compounds. For β -pinene, α -terpineol, and D-

limonene SOA, the H_2O_2 yields from SOA_{O3} are about one order of magnitude higher than those from SOA_{OH} . This is consistent with the reaction mechanism of ozonolysis, in which stabilized Criegee intermediates hydrolyze to form α -hydroxyhydroperoxides that can readily decompose into carbonyls and H_2O_2 . 18,49,50

The distinct profiles of ROS composition by SOA_{O3} and SOA_{OH} reflect differences in chemical compositions and functionalities caused by different oxidation pathways. Monoterpene SOA from ozonolysis generally contain higher fractions of organic peroxides (12–65%) compared to those from photooxidation (6–18%),^{51,52} partly because organic hydroperoxides are decomposed with prolonged UV exposure.^{53,54} As ROOH can be a primary source of *OH radicals through decomposition,^{20,26} lower ROOH fractions should lead to minor contributions of *OH formation for SOA_{OH}. Detailed ROS formation mechanisms are discussed below to better understand how precursors and oxidation systems can affect ROS profiles.

Reaction Mechanism. The temporal evolution of *OH and $O_2^{\bullet-}/HO_2^{\bullet}$ formation from the aqueous reactions of SOA was measured. As shown in Figure 3a, the molar yields of BMPO-OH adducts from SOA_{O3} increase over time and reach a steady state after approximately 2 h. In contrast, the molar yields of BMPO-OOH adducts from SOA_{O3} (except α terpineol SOA_{O3}, which was below detection limit) reach their maximum concentrations within a short period of time (<30 min), followed by a slight decrease (Figure 3b). For SOA_{OH}, O₂•-/HO₂• yields reach their maximum within 40 min, but decrease gradually over 4 h (Figure 3c). The BMPO-OH concentrations from all SOA_{OH} are below the detection limit. The highly distinct time-dependent profiles of ${}^{\bullet}OH$ and $O_2{}^{\bullet-}/$ HO₂ formation lead to an interesting evolution of radical composition by SOA. For example, radical production from isoprene and β -pinene SOA_{O3} is initially dominated by O₂[•]/ HO₂, while OH becomes dominant after 20 min (Figure S3a). In comparison, D-limonene SOA_{O3} and all types of SOA_{OH} (Figure S3b) are consistently dominated by O₂•-/ HO₂ (>70%) over 4 h.

To further elaborate the reaction kinetics and mechanism, a kinetic model was developed and applied to simulate the temporal evolution of ${}^{\bullet}OH$ and $O_2{}^{\bullet-}/HO_2{}^{\bullet}$ radicals. The following reactions were implemented into the kinetic model for ${}^{\bullet}OH$ and $O_2{}^{\bullet-}/HO_2{}^{\bullet}$ formation

$$ROOH \rightarrow RO^{\bullet} + {^{\bullet}OH}$$
 (R1)

$$R_1R_2CHOH + {}^{\bullet}OH \xrightarrow{O_2} c_1R_1R_2C(O_2)OH^{\bullet}$$
 (R2)

$$R_1R_2C(O_2)OH^{\bullet} \rightarrow R_1C(O)R_2 + HO_2^{\bullet}$$
 (R3)

 $^{\bullet}$ OH can be generated from the first-order decay of organic hydroperoxides (ROOH) (R1). 20,26,55 Krapf et al. 10 provided molecular evidence of the unimolecular decomposition of labile hydroperoxides in the condensed phase through the cleavage of the weaker O–O bond which must lead to $^{\bullet}$ OH formation. In addition, direct $^{\bullet}$ OH formation has been observed from the decomposition of cumene hydroperoxide 20 (common proxy of atmospheric ROOH) at room temperature and a recent study 56 and organic radicals. Note that $^{\bullet}$ OH formation in R1 results from the decomposition of organic hydroperoxides without additional functionalities on the α-carbon, as the decomposition of α-hydroxyhydroperoxides leads to the formation of carbonyl and H₂O₂ instead of $^{\bullet}$ OH. 50

The generated ${}^{\bullet}OH$ can abstract a hydrogen atom from α -carbon of primary or secondary alcohols to form α -hydroxyalkyl radicals $(R_1R_2C(OH)^{\bullet})$, which immediately combine with dissolved O_2 to form α -hydroxyperoxyl radicals $(R_1R_2C(O_2)OH)^{\bullet})$ (R2). These radicals can subsequently undergo unimolecular decomposition to form HO_2^{\bullet} (R3). Note that this reaction is known to occur also in the gas phase.

Note that ${}^{\bullet}$ OH formation can be promoted in the presence of transition metal ions via Fenton(-like) reactions. ^{57,58} To address this possible interference of metal contamination on radical formation, concentrations of Fe and Cu ions in the SOA extracts were measured using two highly sensitive spectrophotometric methods (ferrozine and bathocuproine methods, ⁴¹ respectively). The results showed that they were both below the detection limits (10 ± 2 and 20 ± 5 nM for Fe and Cu ions, respectively). An additional control experiment was also conducted for measuring ROS formation from SOA extracts with and without a metal-chelating agent, diethylene-triaminepentaacetic acid, showing no significant difference, confirming the negligible impacts of potential metal contamination.

The kinetic model also considers a number of other reactions including OH loss via reactions with SOA components, ROS coupling reactions, radical trapping by BMPO, and decay of BMPO-radical adducts (Table S2). Molar fractions of ROOH and R₁R₂CHOH contained in SOA were estimated using the MCGA to reproduce experimental data.⁴⁴ The decomposition rate of ROOH estimated in this study ((0.9-6.5) \times 10⁻⁵ s⁻¹) is in agreement with previous studies, 20,28 and the lifetime of α -hydroxyperoxyl radicals (0.002-0.06 s) is also consistent with the aqueous chemistry model CAPRAM 3.0 (0.001-0.005 s). 42 As shown in Figure 3, the modeling results show a good agreement with measurements within modeling uncertainties, indicating that the above reaction mechanisms are plausible for OH and O2 -/HO2 formation as they can explain the temporal evolution of distinct radical profiles depending on precursors and oxidation pathways. It should be noted that the decomposition rates involving hydroperoxides could be pH-dependent according to a recent study by Qiu et al. 59 Therefore, future studies are still warranted for the pH effects on ROS formation from SOA in the aqueous phase, where acidification (representative of aerosol pH) and neutralization (representative of physiological pH) are of interest and could both play a role in affecting the profiles of radical production.

The model-estimated molar fractions of ROOH in isoprene, β -pinene, and D-limonene SOA_{O3} are 6–25, 7–35, and 2– 12%, respectively (Table S3), which are comparable with the peroxide mass fractions reported by previous studies for the same types of SOA (\sim 30, \sim 85, and \sim 2%, respectively), 2,51,60,61 assuming that molar masses of peroxides and SOA components are the same. Note that the measured total peroxide contents include both organic peroxides (ROOR) and hydroperoxides (ROOH), which may explain the lower estimated fraction of ROOH in isoprene and β -pinene compared to literature values. In addition, it may imply that some ROOH may be more stable and do not decompose within the timescale of the experiment, as has been observed for isoprene hydroxyl hydroperoxide in a recent study.⁶² Significantly higher fractions of ROOH are estimated in the isoprene and β -pinene SOA_{O3} compared to their corresponding SOA_{OH} (3-5% and 1-3%), leading to the major

OH/O₃ autoxidation
$$C_xH_yO_{z1}(O-O)_{z2}$$
 $Condensation$ $C_xH_yO_{z1}(O-O)_{z2}$ $Condensation$ $C_xH_yO_{z1}(O-O)_{z2}$ $Condensation$ $Condensation$

Figure 4. Implications of ROS formation by aqueous reactions of biogenic SOA. HOMs and extremely low volatility organic compounds (ELVOCs) are generated by gas-phase oxidation and autoxidation. After condensation, ROS including ${}^{\bullet}OH$, $O_2^{\bullet -}/HO_2^{\bullet}$, and H_2O_2 can be generated via decomposition of organic hydroperoxides, ${}^{\bullet}OH$ oxidation of primary or secondary alcohols, and unimolecular decomposition of α-hydroxyperoxyl radicals and α-hydroxyperoxyhydroperoxides in the aqueous phase. This process has significant implications for chemical aging of SOA in the atmosphere and oxidative stress upon respiratory deposition of SOA particles.

contribution of *OH formation in SOA_{O3}. The molar fractions of R₁R₂CH(OH) in D-limonene SOA are estimated to be higher compared to ROOH, contributing to the O2 •-/HO2dominated profile for both D-limonene SOAO3 and SOAOH. Significant amounts of R₁R₂CH(OH) are predicted in most SOA (34–74%). Primary and secondary alcohols are generated via multigenerational gas-phase oxidation as shown in a number of previous experimental and theoretical studies as summarized in review papers. The α -terpineol SOA_{O3} is estimated to contain a very small fraction of R₁R₂CH(OH) (0.1-1%), leading to the suppression of the $O_2^{\bullet -}/HO_2^{\bullet}$ formation. This is likely caused by the specific position of hydroxy groups in the α -terpineol: tertiary alcohol without α -H for abstraction and subsequently no formation of peroxyl radicals. The predicted very low fraction of R₁R₂CH(OH) in α-terpineol SOA_{O3} is consistent with previous experimental measurements, 64 showing that the primary products (>90%) from α -terpineol ozonolysis only contain tertiary alcohols.

Implications. This work elucidates ROS generation pathways from aqueous reactions of biogenic SOA as presented in Figure 4. Multigenerational atmospheric oxidation and autoxidation of biogenic VOCs by OH and O3 lead to the formation of highly functionalized and extremely low volatility organic compounds, HOMs, and ELVOCs. 8,9 Most of these compounds contain alcohol and hydroperoxide functional groups. After condensation into the particle phase, a fraction of organic hydroperoxides (ROOH) decomposes to form OH, which can act as an ignition step for a cascade of ROS formation pathways. The e-folding times for the ROOH decomposition are estimated to be 4-30 h, which represent average lifetimes for different ROOH compounds; some of them may have shorter timescales, 10,11 while others may be very stable. 65,66 This decomposition process can be accelerated by photolysis 53,54 and Fenton-like reactions of transition metal ions. 20,28,62 We acknowledge a caveat of this work that the particle mass concentrations in the PAM reactor are much higher compared to ambient conditions, leading to more prominent condensation of semi-VOC. However, a recent study⁶⁶ found that the PAM reactor-generated α -pinene SOA contains substantial amounts of particle-phase HOMs, which is consistent with the gas-phase measurements in previous

studies. ^{9,67,68} Although this study serves as a proof of concept and provide mechanistic insights into possible mechanisms of ROS formation, future studies are definitively warranted to investigate the ROS formation from SOA generated under conditions with lower oxidant and particle concentrations.

The ${}^{\bullet}$ OH released during SOA decomposition can abstract hydrogen from primary or secondary alcohols (R₁R₂CH(OH)) to form α -hydroxyalkyl radicals, which quickly react with dissolved oxygen to form α -hydroxyperoxyl radicals. Within milliseconds, α -hydroxyperoxyl radicals can undergo unimolecular decomposition to form $O_2^{\bullet-}/HO_2^{\bullet}$ radicals. Through HO_2^{\bullet} termination, α -hydroxyperoxyl radicals form α -hydroxyalkyl hydroperoxides, which can decompose to generate H_2O_2 , another important ROS. SO,69 Note that α -hydroxyalkyl hydroperoxides can form a stable complex with a water molecule, so the -O-OH group is unlikely to be cleaved to yield ${}^{\bullet}OH$ radicals. SO,70 Other feasible pathways of H_2O_2 formation by SOA have also been discussed in the literature including hydrolysis of diacyl peroxides or peroxy acids, and the relative contributions of different H_2O_2 sources still warrant further studies.

Our findings demonstrate the importance of the interplay among different functionalities in determining radical production in the aqueous phase. The relative abundance of ROOH and R₁R₂CH(OH) can largely affect the compositions of *OH, O2*-/HO2, H2O2, and organic radicals. It has been established that ROS play a central role in chemical transformation of organic and inorganic compounds in aqueous particles. Sources, sinks, and concentrations of ROS in atmospheric waters are still uncertain and it is still challenging to accurately predict their concentrations in atmospheric aqueous chemistry models. 13,72 Implementation of molar yields of ROS by SOA determined in this study into models should improve quantification of ROS in aqueous droplets, which can then be compared with traditional ROS sources such as gaseous HO_x uptake and Fenton reactions to evaluate relative importance of different ROS formation pathways.

 α -Terpineol and D-limonene are known as important indoorrelevant VOCs. α -Terpineol is a significant component of liquid cleaner/disinfectants and air fresheners and can be

emitted by some molds in the indoor environment, whereas p-limonene has been found in floor wax, all-purpose cleaners, and personal care products. These terpenes are found in higher concentrations in indoor environments compared to outdoors and their oxidation can lead to substantial SOA formation indoors. These compounds can also be transported to the outdoors, affecting ozone and SOA formation in the atmosphere. Trepineol SOA_{O3} and p-limonene SOA_{OH} show the highest formation efficiencies in the aqueous generation of OH and $O_2^{\bullet-}/HO_2^{\bullet}$, respectively. Quantification of different types of ROS by SOA should be helpful for a better understanding of the aqueous-phase processing of chemical compounds in indoor and outdoor processes.

Upon inhalation and respiratory deposition of SOA particles, $O_2^{\bullet-}$ can be generated via redox reactions with lung antioxidants or can be released by macrophages after phagocytosis of inhaled particles in the lung-lining fluid. ^{76,77} The antioxidant defense system can counteract ROS, however, excessive production of ROS can overwhelm antioxidant defenses and trigger or enhance oxidative stress, cell death, and biological aging. ^{31,78} As direct measurements of ROS in the lung-lining fluid are challenging, implementation of formation efficiency of $O_2^{\bullet-}$ into the lung model ^{30,32} will improve quantification of ROS in the lung-lining fluid for a better evaluation of the impact of biogenic SOA on oxidative stress and adverse health effects including asthma, allergies, and other respiratory diseases.

ASSOCIATED CONTENT

5 Supporting Information

The Supporting Information is available free of charge at https://pubs.acs.org/doi/10.1021/acs.est.0c07789.

SOA chemistry and $\rm H_2O_2$ fluorometric assay; $\rm H_2O_2$ yields of aqueous reactions or SOA; chemical reactions and parameters in the kinetic model; molar fractions of ROOH and $\rm R_1R_2CHOH$ in SOA; schematics of dark ozonolysis and $^{\bullet}OH$ photooxidation; EPR spectra of BMPO-radical adducts from aqueous reactions of SOA; temporal evolution of relative yields of BMPO-radical adducts from aqueous reactions of SOA; correlation of BMPO-OOH and $\rm H_2O_2$ concentrations in aqueous reactions of SOA (PDF)

AUTHOR INFORMATION

Corresponding Author

Manabu Shiraiwa — Department of Chemistry, University of California, Irvine, California 92697-2025, United States; orcid.org/0000-0003-2532-5373; Email: m.shiraiwa@uci.edu

Authors

Jinlai Wei — Department of Chemistry, University of California, Irvine, California 92697-2025, United States; orcid.org/0000-0002-4741-9015

Ting Fang — Department of Chemistry, University of California, Irvine, California 92697-2025, United States; orcid.org/0000-0002-4845-2749

Cynthia Wong — Department of Chemistry, University of California, Irvine, California 92697-2025, United States Pascale S. J. Lakey — Department of Chemistry, University of California, Irvine, California 92697-2025, United States Sergey A. Nizkorodov — Department of Chemistry, University of California, Irvine, California 92697-2025, United States; orcid.org/0000-0003-0891-0052

Complete contact information is available at: https://pubs.acs.org/10.1021/acs.est.0c07789

Notes

The authors declare no competing financial interest.

ACKNOWLEDGMENTS

The research described in this article was conducted under contract to the Health Effects Institute (HEI) (Walter A. Rosenblith New Investigator Award, no. 4964-RFA17-3/18-6), an organization jointly funded by the United States Environmental Protection Agency (EPA) (Assistance Award no. CR-83590201) and certain motor vehicle and engine manufacturers. The contents of this article neither necessarily reflect the views of HEI, or its sponsors, nor they necessarily reflect the views and policies of the EPA or motor vehicle and engine manufacturers. We also acknowledge funding from the National Science Foundation (CHE-1808125). We acknowledge Prof. William Brune (Pennsylvania State University) for loaning the PAM reactor, Dr. Thomas Berkemeier (Max Planck Institute for Chemistry) for sharing the code of Monte Carlo genetic algorithm and stimulating discussions, and Dr. Tommaso Galeazzo (UC Irvine) for discussions on chemical mechanisms.

REFERENCES

- (1) Shrivastava, M.; Cappa, C. D.; Fan, J.; Goldstein, A. H.; Guenther, A. B.; Jimenez, J. L.; Kuang, C.; Laskin, A.; Martin, S. T.; Ng, N. L.; Petaja, T.; Pierce, J. R.; Rasch, P. J.; Roldin, P.; Seinfeld, J. H.; Shilling, J.; Smith, J. N.; Thornton, J. A.; Volkamer, R.; Wang, J.; Worsnop, D. R.; Zaveri, R. A.; Zelenyuk, A.; Zhang, Q. Recent advances in understanding secondary organic aerosol: Implications for global climate forcing. *Rev. Geophys.* 2017, 55, 509–559.
- (2) Shiraiwa, M.; Ueda, K.; Pozzer, A.; Lammel, G.; Kampf, C. J.; Fushimi, A.; Enami, S.; Arangio, A. M.; Fröhlich-Nowoisky, J.; Fujitani, Y.; Furuyama, A.; Lakey, P. S. J.; Lelieveld, J.; Lucas, K.; Morino, Y.; Pöschl, U.; Takahama, S.; Takami, A.; Tong, H.; Weber, B.; Yoshino, A.; Sato, K. Aerosol Health Effects from Molecular to Global Scales. *Environ. Sci. Technol.* **2017**, *51*, 13545–13567.
- (3) Jimenez, J. L.; Canagaratna, M. R.; Donahue, N. M.; Prevot, A. S. H.; Zhang, Q.; Kroll, J. H.; DeCarlo, P. F.; Allan, J. D.; Coe, H.; Ng, N. L.; Aiken, A. C.; Docherty, K. S.; Ulbrich, I. M.; Grieshop, A. P.; Robinson, A. L.; Duplissy, J.; Smith, J. D.; Wilson, K. R.; Lanz, V. A.; Hueglin, C.; Sun, Y. L.; Tian, J.; Laaksonen, A.; Raatikainen, T.; Rautiainen, J.; Vaattovaara, P.; Ehn, M.; Kulmala, M.; Tomlinson, J. M.; Collins, D. R.; Cubison, M. J.; Dunlea, J.; Huffman, J. A.; Onasch, T. B.; Alfarra, M. R.; Williams, P. I.; Bower, K.; Kondo, Y.; Schneider, J.; Drewnick, F.; Borrmann, S.; Weimer, S.; Demerjian, K.; Salcedo, D.; Cottrell, L.; Griffin, R.; Takami, A.; Miyoshi, T.; Hatakeyama, S.; Shimono, A.; Sun, J. Y.; Zhang, Y. M.; Dzepina, K.; Kimmel, J. R.; Sueper, D.; Jayne, J. T.; Herndon, S. C.; Trimborn, A. M.; Williams, L. R.; Wood, E. C.; Middlebrook, A. M.; Kolb, C. E.; Baltensperger, U.; Worsnop, D. R. Evolution of organic aerosols in the atmosphere. Science 2009, 326, 1525–1529.
- (4) Pöschl, U.; Martin, S. T.; Sinha, B.; Chen, Q.; Gunthe, S. S.; Huffman, J. A.; Borrmann, S.; Farmer, D. K.; Garland, R. M.; Helas, G.; Jimenez, J. L.; King, S. M.; Manzi, A.; Mikhailov, E.; Pauliquevis, T.; Petters, M. D.; Prenni, A. J.; Roldin, P.; Rose, D.; Schneider, J.; Su, H.; Zorn, S. R.; Artaxo, P.; Andreae, M. O. Rainforest aerosols as biogenic nuclei of clouds and precipitation in the Amazon. *Science* 2010, 329, 1513–1516.
- (5) Huang, R.-J.; Zhang, Y.; Bozzetti, C.; Ho, K.-F.; Cao, J.-J.; Han, Y.; Daellenbach, K. R.; Slowik, J. G.; Platt, S. M.; Canonaco, F.;

- Zotter, P.; Wolf, R.; Pieber, S. M.; Bruns, E. A.; Crippa, M.; Ciarelli, G.; Piazzalunga, A.; Schwikowski, M.; Abbaszade, G.; Schnelle-Kreis, J.; Zimmermann, R.; An, Z.; Szidat, S.; Baltensperger, U.; Haddad, I. E.; Prévôt, A. S. H. High secondary aerosol contribution to particulate pollution during haze events in China. *Nature* **2014**, *514*, 218–222.
- (6) Carlton, A. G.; de Gouw, J.; Jimenez, J. L.; Ambrose, J. L.; Attwood, A. R.; Brown, S.; Baker, K. R.; Brock, C.; Cohen, R. C.; Edgerton, S.; Farkas, C. M.; Farmer, D.; Goldstein, A. H.; Gratz, L.; Guenther, A.; Hunt, S.; Jaeglé, L.; Jaffe, D. A.; Mak, J.; McClure, C.; Nenes, A.; Nguyen, T. K.; Pierce, J. R.; de Sa, S.; Selin, N. E.; Shah, V.; Shaw, S.; Shepson, P. B.; Song, S.; Stutz, J.; Surratt, J. D.; Turpin, B. J.; Warneke, C.; Washenfelder, R. A.; Wennberg, P. O.; Zhou, X. Synthesis of the Southeast Atmosphere Studies: Investigating Fundamental Atmospheric Chemistry Questions. *Bull. Am. Meteorol. Soc.* 2018, 99, 547–567.
- (7) Ziemann, P. J.; Atkinson, R. Kinetics, products, and mechanisms of secondary organic aerosol formation. *Chem. Soc. Rev.* **2012**, *41*, 6582–6605.
- (8) Bianchi, F.; Kurtén, T.; Riva, M.; Mohr, C.; Rissanen, M. P.; Roldin, P.; Berndt, T.; Crounse, J. D.; Wennberg, P. O.; Mentel, T. F.; Wildt, J.; Junninen, H.; Jokinen, T.; Kulmala, M.; Worsnop, D. R.; Thornton, J. A.; Donahue, N.; Kjaergaard, H. G.; Ehn, M. Highly Oxygenated Organic Molecules (HOM) from Gas-Phase Autoxidation Involving Peroxy Radicals: A Key Contributor to Atmospheric Aerosol. *Chem. Rev.* 2019, 119, 3472—3509.
- (9) Ehn, M.; Thornton, J. A.; Kleist, E.; Sipilä, M.; Junninen, H.; Pullinen, I.; Springer, M.; Rubach, F.; Tillmann, R.; Lee, B.; Lopez-Hilfiker, F.; Andres, S.; Acir, I.-H.; Rissanen, M.; Jokinen, T.; Schobesberger, S.; Kangasluoma, J.; Kontkanen, J.; Nieminen, T.; Kurtén, T.; Nielsen, L. B.; Jørgensen, S.; Kjaergaard, H. G.; Canagaratna, M.; Maso, M. D.; Berndt, T.; Petäjä, T.; Wahner, A.; Kerminen, V.-M.; Kulmala, M.; Worsnop, D. R.; Wildt, J.; Mentel, T. F. A large source of low-volatility secondary organic aerosol. *Nature* 2014, 506, 476–479.
- (10) Krapf, M.; El Haddad, I.; Bruns, E. A.; Molteni, U.; Daellenbach, K. R.; Prévôt, A. S. H.; Baltensperger, U.; Dommen, J. Labile Peroxides in Secondary Organic Aerosol. *Chem.* **2016**, *1*, 603–616.
- (11) Pospisilova, V.; Lopez-Hilfiker, F. D.; Bell, D. M.; El Haddad, I.; Mohr, C.; Huang, W.; Heikkinen, L.; Xiao, M.; Dommen, J.; Prevot, A. S. H.; Baltensperger, U.; Slowik, J. G. On the fate of oxygenated organic molecules in atmospheric aerosol particles. *Sci. Adv.* **2020**, *6*, No. eaax8922.
- (12) Ervens, B.; Turpin, B. J.; Weber, R. J. Secondary organic aerosol formation in cloud droplets and aqueous particles (aqSOA): a review of laboratory, field and model studies. *Atmos. Chem. Phys.* **2011**, *11*, 11069–11102.
- (13) Herrmann, H.; Schaefer, T.; Tilgner, A.; Styler, S. A.; Weller, C.; Teich, M.; Otto, T. Tropospheric Aqueous-Phase Chemistry: Kinetics, Mechanisms, and Its Coupling to a Changing Gas Phase. *Chem. Rev.* **2015**, *115*, 4259–4334.
- (14) McNeill, V. F. Aqueous Organic Chemistry in the Atmosphere: Sources and Chemical Processing of Organic Aerosols. *Environ. Sci. Technol.* **2015**, 49, 1237–1244.
- (15) Farmer, D. K.; Cappa, C. D.; Kreidenweis, S. M. Atmospheric Processes and Their Controlling Influence on Cloud Condensation Nuclei Activity. *Chem. Rev.* **2015**, *115*, 4199–4217.
- (16) Laskin, A.; Laskin, J.; Nizkorodov, S. A. Chemistry of Atmospheric Brown Carbon. *Chem. Rev.* **2015**, *115*, 4335–4382.
- (17) Pöschl, U.; Shiraiwa, M. Multiphase Chemistry at the Atmosphere-Biosphere Interface Influencing Climate and Public Health in the Anthropocene. *Chem. Rev.* **2015**, *115*, 4440–4475.
- (18) Wang, Y.; Kim, H.; Paulson, S. E. Hydrogen peroxide generation from α and β -pinene and toluene secondary organic aerosols. *Atmos. Environ.* **2011**, *45*, 3149–3156.
- (19) Gallimore, P. J.; Mahon, B. M.; Wragg, F. P. H.; Fuller, S. J.; Giorio, C.; Kourtchev, I.; Kalberer, M. Multiphase composition changes and reactive oxygen species formation during limonene

- oxidation in the new Cambridge Atmospheric Simulation Chamber (CASC). Atmos. Chem. Phys. 2017, 17, 9853-9868.
- (20) Tong, H.; Arangio, A. M.; Lakey, P. S. J.; Berkemeier, T.; Liu, F.; Kampf, C. J.; Brune, W. H.; Pöschl, U.; Shiraiwa, M. Hydroxyl radicals from secondary organic aerosol decomposition in water. *Atmos. Chem. Phys.* **2016**, *16*, 1761–1771.
- (21) Paulson, S. E.; Gallimore, P. J.; Kuang, X. B. M.; Chen, J. R.; Kalberer, M.; Gonzalez, D. H., A light-driven burst of hydroxyl radicals dominates oxidation chemistry in newly activated cloud droplets. *Sci. Adv.* **2019**, *5*, (). DOI: 10.1126/sciadv.aav7689
- (22) Tong, H.; Zhang, Y.; Filippi, A.; Wang, T.; Li, C.; Liu, F.; Leppla, D.; Kourtchev, I.; Wang, K.; Keskinen, H.-M.; Levula, J. T.; Arangio, A. M.; Shen, F.; Ditas, F.; Martin, S. T.; Artaxo, P.; Godoi, R. H. M.; Yamamoto, C. I.; de Souza, R. A. F.; Huang, R.-J.; Berkemeier, T.; Wang, Y.; Su, H.; Cheng, Y.; Pope, F. D.; Fu, P.; Yao, M.; Pöhlker, C.; Petäjä, T.; Kulmala, M.; Andreae, M. O.; Shiraiwa, M.; Pöschl, U.; Hoffmann, T.; Kalberer, M. Radical Formation by Fine Particulate Matter Associated with Highly Oxygenated Molecules. *Environ. Sci. Technol.* 2019, 53, 12506–12518.
- (23) Kaur, R.; Anastasio, C. Light absorption and the photoformation of hydroxyl radical and singlet oxygen in fog waters. *Atmos. Environ.* **2017**, *164*, 387–397.
- (24) Manfrin, A.; Nizkorodov, S. A.; Malecha, K. T.; Getzinger, G. J.; McNeill, K.; Borduas-Dedekind, N. Reactive Oxygen Species Production from Secondary Organic Aerosols: The Importance of Singlet Oxygen. *Environ. Sci. Technol.* **2019**, *53*, 8553–8562.
- (25) McWhinney, R. D.; Zhou, S.; Abbatt, J. P. D. Naphthalene SOA: redox activity and naphthoquinone gas—particle partitioning. *Atmos. Chem. Phys.* **2013**, *13*, 9731—9744.
- (26) Tong, H.; Lakey, PSJ; Arangio, AM; Socorro, J.; Shen, F.; Lucas, K.; Brune, WH; Pöschl, U.; Shiraiwa, M. Reactive Oxygen Species Formed by Secondary Organic Aerosols in Water and Surrogate Lung Fluid. *Environ. Sci. Technol.* **2018**, *52*, 11642–11651.
- (27) Chowdhury, P. H.; He, Q.; Carmieli, R.; Li, C.; Rudich, Y.; Pardo, M. Connecting the Oxidative Potential of Secondary Organic Aerosols with Reactive Oxygen Species in Exposed Lung Cells. *Environ. Sci. Technol.* **2019**, *53*, 13949–13958.
- (28) Tong, H.; Lakey, P. S. J.; Arangio, A. M.; Socorro, J.; Kampf, C. J.; Berkemeier, T.; Brune, W. H.; Pöschl, U.; Shiraiwa, M. Reactive oxygen species formed in aqueous mixtures of secondary organic aerosols and mineral dust influencing cloud chemistry and public health in the Anthropocene. *Faraday Discuss.* **2017**, 200, 251–270.
- (29) Tuet, W. Y.; Chen, Y.; Xu, L.; Fok, S.; Gao, D.; Weber, R. J.; Ng, N. L. Chemical oxidative potential of secondary organic aerosol (SOA) generated from the photooxidation of biogenic and anthropogenic volatile organic compounds. *Atmos. Chem. Phys.* **2017**, *17*, 839–853.
- (30) Fang, T.; Lakey, P. S. J.; Weber, R. J.; Shiraiwa, M. Oxidative Potential of Particulate Matter and Generation of Reactive Oxygen Species in Epithelial Lining Fluid. *Environ. Sci. Technol.* **2019**, 53, 12784–12792.
- (31) Nel, A. Air Pollution-Related Illness: Effects of Particles. *Science* **2005**, *308*, 804–806.
- (32) Lakey, P. S. J.; Berkemeier, T.; Tong, H.; Arangio, A. M.; Lucas, K.; Pöschl, U.; Shiraiwa, M. Chemical exposure-response relationship between air pollutants and reactive oxygen species in the human respiratory tract. *Sci. Rep.* **2016**, *6*, 32916.
- (33) Kelly, F. J. Oxidative stress: Its role in air pollution and adverse health effects. *Occup. Environ. Med.* **2003**, *60*, 612–616.
- (34) McCord, J. M. The evolution of free radicals and oxidative stress. Am. J. Med. 2000, 108, 652-659.
- (35) Hayyan, M.; Hashim, M. A.; AlNashef, I. M. Superoxide Ion: Generation and Chemical Implications. *Chem. Rev.* **2016**, *116*, 3029–3085.
- (36) Charrier, J. G.; Anastasio, C. Rates of Hydroxyl Radical Production from Transition Metals and Quinones in a Surrogate Lung Fluid. *Environ. Sci. Technol.* **2015**, *49*, 9317–9325.

- (37) Kang, E.; Root, M. J.; Toohey, D. W.; Brune, W. H. Introducing the concept of Potential Aerosol Mass (PAM). *Atmos. Chem. Phys.* **2007**, *7*, 5727–5744.
- (38) Lambe, A. T.; Chhabra, P. S.; Onasch, T. B.; Brune, W. H.; Hunter, J. F.; Kroll, J. H.; Cummings, M. J.; Brogan, J. F.; Parmar, Y.; Worsnop, D. R.; Kolb, C. E.; Davidovits, P. Effect of oxidant concentration, exposure time, and seed particles on secondary organic aerosol chemical composition and yield. *Atmos. Chem. Phys.* **2015**, *15*, 3063–3075.
- (39) Lambe, A. T.; Ahern, A. T.; Williams, L. R.; Slowik, J. G.; Wong, J. P. S.; Abbatt, J. P. D.; Brune, W. H.; Ng, N. L.; Wright, J. P.; Croasdale, D. R.; Worsnop, D. R.; Davidovits, P.; Onasch, T. B. Characterization of aerosol photooxidation flow reactors: heterogeneous oxidation, secondary organic aerosol formation and cloud condensation nuclei activity measurements. *Atmos. Meas. Tech.* **2011**, *4*, 445–461.
- (40) Peng, Z.; Jimenez, J. L. Radical chemistry in oxidation flow reactors for atmospheric chemistry research. *Chem. Soc. Rev.* **2020**, *49*, 2570–2616
- (41) Wei, J.; Yu, H.; Wang, Y.; Verma, V. Complexation of Iron and Copper in Ambient Particulate Matter and Its Effect on the Oxidative Potential Measured in a Surrogate Lung Fluid. *Environ. Sci. Technol.* **2019**, *53*, 1661–1671.
- (42) Herrmann, H.; Tilgner, A.; Barzaghi, P.; Majdik, Z.; Gligorovski, S.; Poulain, L.; Monod, A. Towards a more detailed description of tropospheric aqueous phase organic chemistry: CAPRAM 3.0. Atmos. Environ. 2005, 39, 4351–4363.
- (43) Bothe, E.; Schuchmann, M. N.; Schulte-Frohlinde, D.; von Sonntag, C. v. HO₂ Elimination from Alpha-Hydroxyalkylperoxyl Radicals in Aqueous-Solution. *Photochem. Photobiol.* **1978**, 28, 639–643.
- (44) Berkemeier, T.; Ammann, M.; Krieger, U. K.; Peter, T.; Spichtinger, P.; Pöschl, U.; Shiraiwa, M.; Huisman, A. J. Technical note: Monte Carlo genetic algorithm (MCGA) for model analysis of multiphase chemical kinetics to determine transport and reaction rate coefficients using multiple experimental data sets. *Atmos. Chem. Phys.* 2017, 17, 8021–8029.
- (45) Tresp, H.; Hammer, M. U.; Winter, J.; Weltmann, K. D.; Reuter, S. Quantitative detection of plasma-generated radicals in liquids by electron paramagnetic resonance spectroscopy. *J. Phys. D: Appl. Phys.* **2013**, *46*, 435401.
- (46) Biller, J. R.; Tseitlin, M.; Mitchell, D. G.; Yu, Z.; Buchanan, L. A.; Elajaili, H.; Rosen, G. M.; Kao, J. P. Y.; Eaton, S. S.; Eaton, G. R. Improved Sensitivity for Imaging Spin Trapped Hydroxyl Radical at 250 MHz. *ChemPhysChem* **2015**, *16*, 528–531.
- (47) Mitchell, D. G.; Rosen, G. M.; Tseitlin, M.; Symmes, B.; Eaton, S. S.; Eaton, G. R. Use of Rapid-Scan EPR to Improve Detection Sensitivity for Spin-Trapped Radicals. *Biophys. J.* **2013**, *105*, 338–342.
- (48) Twahir, U. T.; Stedwell, C. N.; Lee, C. T.; Richards, N. G. J.; Polfer, N. C.; Angerhofer, A. Observation of superoxide production during catalysis of Bacillus subtilis oxalate decarboxylase at pH 4. Free Radic. Biol. Med. 2015, 80, 59–66.
- (49) Hasson, A. S.; Ho, A. W.; Kuwata, K. T.; Paulson, S. E. Production of stabilized Criegee intermediates and peroxides in the gas phase ozonolysis of alkenes 2. Asymmetric and biogenic alkenes. *J. Geophys. Res. Atmos.* **2001**, *106*, 34143–34153.
- (50) Qiu, J.; Liang, Z.; Tonokura, K.; Colussi, A. J.; Enami, S. Stability of Monoterpene-Derived α -Hydroxyalkyl-Hydroperoxides in Aqueous Organic Media: Relevance to the Fate of Hydroperoxides in Aerosol Particle Phases. *Environ. Sci. Technol.* **2020**, *54*, 3890–3899.
- (51) Docherty, K. S.; Wu, W.; Lim, Y. B.; Ziemann, P. J. Contributions of organic peroxides to secondary aerosol formed from reactions of monoterpenes with O₃. *Environ. Sci. Technol.* **2005**, 39, 4049–4059.
- (52) Mertes, P.; Pfaffenberger, L.; Dommen, J.; Kalberer, M.; Baltensperger, U. Development of a sensitive long path absorption photometer to quantify peroxides in aerosol particles (Peroxide-LOPAP). *Atmos. Meas. Tech.* **2012**, *5*, 2339–2348.

- (53) Epstein, S. A.; Blair, S. L.; Nizkorodov, S. A. Direct photolysis of α -pinene ozonolysis secondary organic aerosol: effect on particle mass and peroxide content. *Environ. Sci. Technol.* **2014**, *48*, 11251–11258
- (54) Badali, K. M.; Zhou, S.; Aljawhary, D.; Antiñolo, M.; Chen, W. J.; Lok, A.; Mungall, E.; Wong, J. P. S.; Zhao, R.; Abbatt, J. P. D. Formation of hydroxyl radicals from photolysis of secondary organic aerosol material. *Atmos. Chem. Phys.* **2015**, *15*, 7831–7840.
- (55) Chen, Q.; Liu, Y.; Donahue, N. M.; Shilling, J. E.; Martin, S. T. Particle-Phase Chemistry of Secondary Organic Material: Modeled Compared to Measured O:C and H:C Elemental Ratios Provide Constraints. *Environ. Sci. Technol.* **2011**, 45, 4763–4770.
- (56) Tilgner, A.; Herrmann, H., Tropospheric Aqueous-Phase OH Oxidation Chemistry: Current Understanding, Uptake of Highly Oxidized Organics and Its Effects. In *Multiphase Environmental Chemistry in the Atmosphere*; American Chemical Society: 2018; Vol. 1299, pp 49–85.
- (57) Chevallier, E.; Jolibois, R. D.; Meunier, N.; Carlier, P.; Monod, A. "Fenton-like" reactions of methylhydroperoxide and ethylhydroperoxide with Fe²⁺ in liquid aerosols under tropospheric conditions. *Atmos. Environ.* **2004**, *38*, 921–933.
- (58) Nam, W.; Han, H. J.; Oh, S.-Y.; Lee, Y. J.; Choi, M.-H.; Han, S.-Y.; Kim, C.; Woo, S. K.; Shin, W. New Insights into the Mechanisms of O–O Bond Cleavage of Hydrogen Peroxide and tert-Alkyl Hydroperoxides by Iron(III) Porphyrin Complexes. *J. Am. Chem. Soc.* 2000, 122, 8677–8684.
- (59) Qiu, J.; Tonokura, K.; Enami, S. Proton-Catalyzed Decomposition of α -Hydroxyalkyl-Hydroperoxides in Water. *Environ. Sci. Technol.* **2020**, *54*, 10561–10569.
- (60) Nguyen, T. B.; Bateman, A. P.; Bones, D. L.; Nizkorodov, S. A.; Laskin, J.; Laskin, A. High-resolution mass spectrometry analysis of secondary organic aerosol generated by ozonolysis of isoprene. *Atmos. Environ.* **2010**, *44*, 1032–1042.
- (61) Bateman, A. P.; Nizkorodov, S. A.; Laskin, J.; Laskin, A. Photolytic processing of secondary organic aerosols dissolved in cloud droplets. *Phys. Chem. Chem. Phys.* **2011**, *13*, 12199–12212.
- (62) Fang, T.; Lakey, P. S. J.; Rivera-Rios, J. C.; Keutsch, F. N.; Shiraiwa, M. Aqueous-Phase Decomposition of Isoprene Hydroxy Hydroperoxide and Hydroxyl Radical Formation by Fenton-Like Reactions with Iron Ions. *J. Phys. Chem. A* **2020**, 124, 5230–5236.
- (63) Vereecken, L.; Francisco, J. S. Theoretical studies of atmospheric reaction mechanisms in the troposphere. *Chem. Soc. Rev.* **2012**, *41*, 6259–6293.
- (64) Leviss, D. H.; Van Ry, D. A.; Hinrichs, R. Z. Multiphase Ozonolysis of Aqueous α -Terpineol. *Environ. Sci. Technol.* **2016**, *50*, 11698–11705.
- (65) Kenseth, C. M.; Huang, Y.; Zhao, R.; Dalleska, N. F.; Hethcox, J. C.; Stoltz, B. M.; Seinfeld, J. H. Synergistic O_3 + OH oxidation pathway to extremely low-volatility dimers revealed in β -pinene secondary organic aerosol. *Proc. Natl. Acad. Sci. U.S.A.* **2018**, *115*, 8301.
- (66) Zhang, X.; Lambe, A. T.; Upshur, M. A.; Brooks, W. A.; Gray Bé, A.; Thomson, R. J.; Geiger, F. M.; Surratt, J. D.; Zhang, Z.; Gold, A.; Graf, S.; Cubison, M. J.; Groessl, M.; Jayne, J. T.; Worsnop, D. R.; Canagaratna, M. R. Highly Oxygenated Multifunctional Compounds in α-Pinene Secondary Organic Aerosol. *Environ. Sci. Technol.* **2017**, *51*, 5932–5940.
- (67) Ehn, M.; Kleist, E.; Junninen, H.; Petäjä, T.; Lönn, G.; Schobesberger, S.; Dal Maso, M.; Trimborn, A.; Kulmala, M.; Worsnop, D. R.; Wahner, A.; Wildt, J.; Mentel, T. F. Gas phase formation of extremely oxidized pinene reaction products in chamber and ambient air. *Atmos. Chem. Phys.* **2012**, *12*, 5113–5127.
- (68) Kirkby, J.; Duplissy, J.; Sengupta, K.; Frege, C.; Gordon, H.; Williamson, C.; Heinritzi, M.; Simon, M.; Yan, C.; Almeida, J.; Tröstl, J.; Nieminen, T.; Ortega, I. K.; Wagner, R.; Adamov, A.; Amorim, A.; Bernhammer, A.-K.; Bianchi, F.; Breitenlechner, M.; Brilke, S.; Chen, X.; Craven, J.; Dias, A.; Ehrhart, S.; Flagan, R. C.; Franchin, A.; Fuchs, C.; Guida, R.; Hakala, J.; Hoyle, C. R.; Jokinen, T.; Junninen, H.; Kangasluoma, J.; Kim, J.; Krapf, M.; Kürten, A.; Laaksonen, A.;

- Lehtipalo, K.; Makhmutov, V.; Mathot, S.; Molteni, U.; Onnela, A.; Peräkylä, O.; Piel, F.; Petäjä, T.; Praplan, A. P.; Pringle, K.; Rap, A.; Richards, N. A. D.; Riipinen, I.; Rissanen, M. P.; Rondo, L.; Sarnela, N.; Schobesberger, S.; Scott, C. E.; Seinfeld, J. H.; Sipilä, M.; Steiner, G.; Stozhkov, Y.; Stratmann, F.; Tomé, A.; Virtanen, A.; Vogel, A. L.; Wagner, A. C.; Wagner, P. E.; Weingartner, E.; Wimmer, D.; Winkler, P. M.; Ye, P.; Zhang, X.; Hansel, A.; Dommen, J.; Donahue, N. M.; Worsnop, D. R.; Baltensperger, U.; Kulmala, M.; Carslaw, K. S.; Curtius, J. Ion-induced nucleation of pure biogenic particles. *Nature* **2016**, 533, 521–526.
- (69) Sauer, F.; Schäfer, C.; Neeb, P.; Horie, O.; Moortgat, G. K. Formation of hydrogen peroxide in the ozonolysis of isoprene and simple alkenes under humid conditions. *Atmos. Environ.* **1999**, 33, 229–241.
- (70) Kumar, M.; Busch, D. H.; Subramaniam, B.; Thompson, W. H. Role of Tunable Acid Catalysis in Decomposition of α -Hydroxyalkyl Hydroperoxides and Mechanistic Implications for Tropospheric Chemistry. *J. Phys. Chem. A* **2014**, *118*, 9701–9711.
- (71) Ziemann, P. J. Evidence for Low-Volatility Diacyl Peroxides as a Nucleating Agent and Major Component of Aerosol Formed from Reactions of O₃ with Cyclohexene and Homologous Compounds. *J. Phys. Chem. A* **2002**, *106*, 4390–4402.
- (72) Arakaki, T.; Anastasio, C.; Kuroki, Y.; Nakajima, H.; Okada, K.; Kotani, Y.; Handa, D.; Azechi, S.; Kimura, T.; Tsuhako, A.; Miyagi, Y. A General Scavenging Rate Constant for Reaction of Hydroxyl Radical with Organic Carbon in Atmospheric Waters. *Environ. Sci. Technol.* **2013**, *47*, 8196–8203.
- (73) Nazaroff, W. W.; Weschler, C. J. Cleaning products and air fresheners: exposure to primary and secondary air pollutants. *Atmos. Environ.* **2004**, 38, 2841–2865.
- (74) Waring, M. S. Secondary organic aerosol in residences: predicting its fraction of fine particle mass and determinants of formation strength. *Indoor Air* **2014**, *24*, 376–389.
- (75) McDonald, B. C.; de Gouw, J. A.; Gilman, J. B.; Jathar, S. H.; Akherati, A.; Cappa, C. D.; Jimenez, J. L.; Lee-Taylor, J.; Hayes, P. L.; McKeen, S. A.; Cui, Y. Y.; Kim, S.-W.; Gentner, D. R.; Isaacman-VanWertz, G.; Goldstein, A. H.; Harley, R. A.; Frost, G. J.; Roberts, J. M.; Ryerson, T. B.; Trainer, M. Volatile chemical products emerging as largest petrochemical source of urban organic emissions. *Science* **2018**, *359*, 760.
- (76) Kleinman, M. T.; Sioutas, C.; Chang, M. C.; Boere, A. J. F.; Cassee, F. R. Ambient fine and coarse particle suppression of alveolar macrophage functions. *Toxicol. Lett.* **2003**, *137*, 151–158.
- (77) Becker, S.; Soukup, J. M.; Gilmour, M. I.; Devlin, R. B. Stimulation of Human and Rat Alveolar Macrophages by Urban Air Particulates: Effects on Oxidant Radical Generation and Cytokine Production. *Toxicol. Appl. Pharmacol.* **1996**, *141*, 637–648.
- (78) Winterbourn, C. C. Reconciling the chemistry and biology of reactive oxygen species. *Nat. Chem. Biol.* **2008**, *4*, 278–286.